RNA (2000), *6*:311–324. Cambridge University Press. Printed in the USA.

An unusual structure formed by antisense-target RNA binding involves an extended kissing complex with a four-way junction and a side-by-side helical alignment

FABRICE A. KOLB,[1] CHARLOTTA MALMGREN,[3] ERIC WESTHOF,[1] CHANTAL EHRESMANN,[1] BERNARD EHRESMANN,[1] E. GERHART H. WAGNER,[2] and PASCALE ROMBY[1]

[1]UPR 9002 du Centre National de la Recherche Scientifique, Institut de Biologie Moléculaire et Cellulaire, 15 rue R. Descartes, Strasbourg cedex, France
[2]Department of Microbiology, SLU (Swedish University of Agricultural Sciences), Genetikvägen 5, S-75007 Uppsala, Sweden
[3]Department of Microbiology, Biomedical Center, Uppsala University, S-751 23 Uppsala, Sweden

ABSTRACT

The antisense RNA CopA binds to the leader region of the *repA* mRNA (target: CopT). Previous studies on CopA–CopT pairing in vitro showed that the dominant product of antisense RNA–mRNA binding is not a full RNA duplex. We have studied here the structure of CopA–CopT complex, combining chemical and enzymatic probing and computer graphic modeling. CopI, a truncated derivative of CopA unable to bind CopT stably, was also analyzed. We show here that after initial loop–loop interaction (kissing), helix propagation resulted in an extended kissing complex that involves the formation of two intermolecular helices. By introducing mutations (base-pair inversions) into the upper stem regions of CopA and CopT, the boundaries of the two newly formed intermolecular helices were delimited. The resulting extended kissing complex represents a new type of four-way junction structure that adopts an asymmetrical X-shaped conformation formed by two helical domains, each one generated by coaxial stacking of two helices. This structure motif induces a side-by-side alignment of two long intramolecular helices that, in turn, facilitates the formation of an additional intermolecular helix that greatly stabilizes the inhibitory CopA–CopT RNA complex. This stabilizer helix cannot form in CopI–CopT complexes due to absence of the sequences involved. The functional significance of the three-dimensional models of the extended kissing complex (CopI–CopT) and the stable complex (CopA–CopT) are discussed.

Keywords: antisense RNA; chemical mapping; RNA modeling; RNA–RNA interaction; RNA structure

INTRODUCTION

Many untranslated RNAs exert regulatory functions in both prokaryotes and eukaryotes. A subclass of these regulators, called antisense RNAs, affects target RNA function via binding to complementary sequences. Most antisense RNAs have been identified in prokaryotic cells, mainly in their plasmids, transposons, and bacteriophages (reviewed by Wagner & Simons, 1994; Wagner & Brantl, 1998; Zeiler & Simons, 1998). Plasmid R1 belongs to the IncFII group of plasmids whose initiation frequency is controlled by an antisense RNA, CopA. Synthesis of the replication initiator protein RepA requires translation of a short leader peptide (*tap*), located upstream of *repA.* CopA binds to the leader region of the *repA* mRNA (CopT), located about 80 nt upstream of the *repA* start codon (Fig. 1). Binding prevents *tap* translation and thereby *repA* expression (Blomberg et al., 1992, 1994; Malmgren et al., 1996). The CopA–CopT binding process is viewed as a series of reactions leading to progressively more stable complexes (Persson et al., 1988, 1990a, 1990b; Malmgren et al., 1997). CopA and CopT are fully complementary and both RNAs contain a major stem-loop structure (II/II′ in Fig. 1) that is essential for high pairing rates

Reprint requests to: Pascale Romby, UPR 9002 du Centre National de la Recherche Scientifique, Institut de Biologie Moléculaire et Cellulaire, 15 rue R. Descartes, Strasbourg cedex, France; e-mail: P.Romby@ibmc.U-strasbg.fr; or E. Gerhart H. Wagner, Department of Microbiology, SLU (Swedish University of Agricultural Sciences), Box 7025, Genetikvägen 5, S-75007 Uppsala, Sweden; e-mail: gerhart.wagner@mikrob.slu.se.

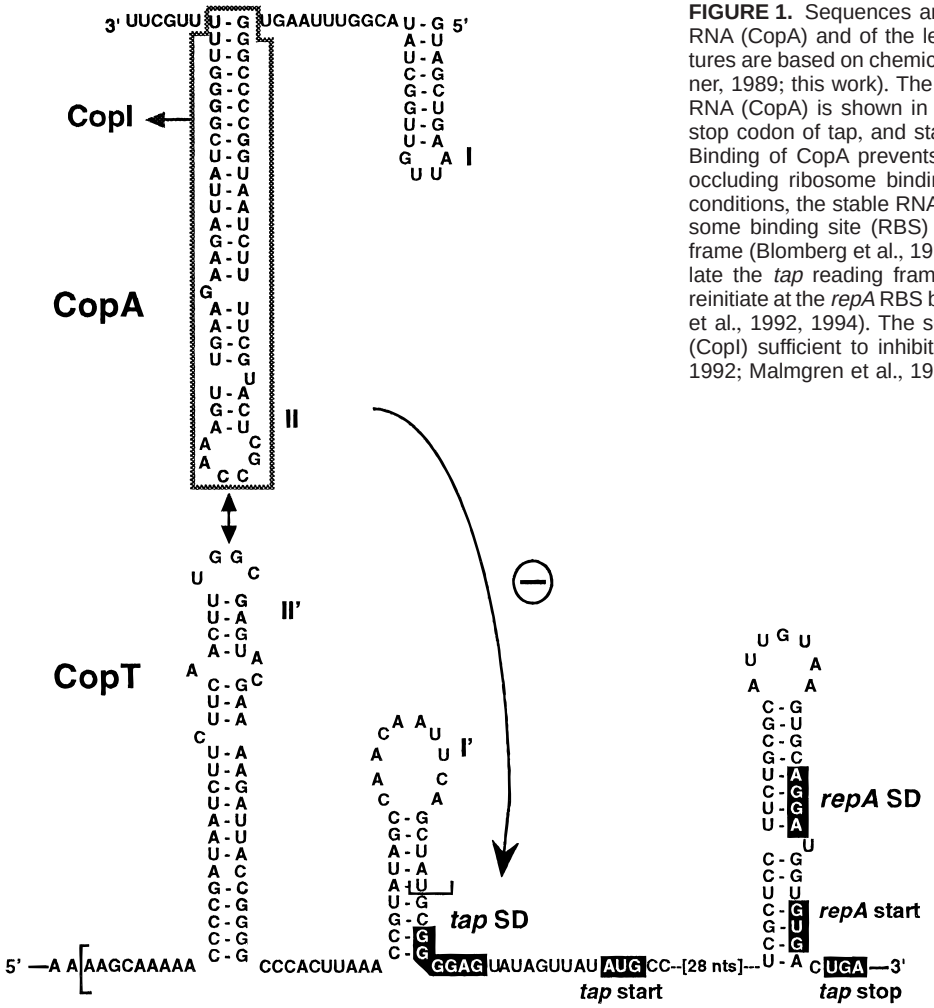

FIGURE 1. Sequences and secondary structures of the antisense RNA (CopA) and of the leader segment of the *repA* mRNA. Structures are based on chemical and enzymatic probing (Öhman & Wagner, 1989; this work). The target sequence (CopT) of the antisense RNA (CopA) is shown in brackets. The Shine and Dalgarno (SD), stop codon of tap, and start codons of *tap* and *repA* are indicated. Binding of CopA prevents translation of the *tap* reading frame by occluding ribosome binding at *tap* initiation site (−). Under these conditions, the stable RNA stem-loop that sequesters the *repA* ribosome binding site (RBS) prevents translation of the *repA* reading frame (Blomberg et al., 1994). If CopA fails to bind, ribosomes translate the *tap* reading frame, terminate at the *tap* stop codon, and reinitiate at the *repA* RBS by a direct translational coupling (Blomberg et al., 1992, 1994). The sequence of the truncated antisense RNA (CopI) sufficient to inhibit *tap* translation is boxed (Wagner et al., 1992; Malmgren et al., 1996).

and control (Öhman & Wagner, 1989; Hjalt & Wagner, 1992, 1995). The initial step involves a transient loop–loop interaction (kissing complex) between the complementary hairpin loops (Persson et al., 1990a, 1990b). Indeed, a truncated CopA (CopI, Fig. 1), lacking the 5′ proximal 30 nt and consisting only of the major stem-loop, does not form stable duplexes with CopT, but is capable of competing with CopA for binding (Persson et al., 1990b). It was recently shown that in both CopI–CopT and CopA–CopT complexes, initial kissing is rapidly followed by more extended intermolecular interactions (Malmgren et al., 1997). Subsequently, the single-stranded region in the 5′ tail of CopA pairs with its complement in CopT to yield the stable, inhibitory CopA–CopT complex. This complex is the dominant product of binding in vitro (Malmgren et al., 1996, 1997). Complete duplex formation is very slow and has been proposed to be irrelevant for control (Malmgren et al., 1996, 1997; Wagner & Brantl, 1998).

Different pairing pathways that result in rapid formation of stable antisense-target RNA complexes have been described (Kittle et al., 1989; Persson et al., 1990b; Tomizawa, 1990; Siemering et al., 1994; Thisted et al., 1994). A common feature is the use of a restricted single-stranded region in each interacting RNA for the initial step. In most cases, binding initiates between two loops, in some cases between a loop and a single-stranded RNA segment. Subsequently, more stable complexes are either formed by the pairing of distal RNA segments or, in the latter case, by extension of the first helix.

In the plasmids of the ColE1-family, control of replication is mediated by an antisense RNA, RNAI, that interacts with the preprimer, RNAII, via initial and transient base pairing between complementary loops (Eguchi et al., 1991; Eguchi & Tomizawa, 1991). NMR studies were performed on two RNA hairpins carrying seven-membered complementary loops derived from RNAI/RNAII (Marino et al., 1995; Lee & Crothers, 1998). These studies indicated that all seven loop bases were paired in the loop–loop helix, and continuous stacking of the loop nucleotides on the 3′ side of their respective stems was observed. Loop–loop interactions in plasmid R1 (IncFII plasmid; Persson et al., 1990a, 1990b; Malmgren et al., 1997), pMU720 (IncB plasmid; Siemering et al., 1994), and ColIb-P9 (IncIα plasmid; Asano et al., 1998)

are clearly similar. In all these systems, it was suggested that an initial loop–loop interaction is rapidly converted to an extended kissing complex. This requires partial melting of the upper stem regions, most probably facilitated by the presence of bulged residues (Siemering et al., 1994; Hjalt & Wagner, 1995). Interestingly, the extended kissing complex suffices for inhibition in vivo (Wagner et al., 1992; Wilson et al., 1993). In the case of plasmid R1, the extended kissing complex is also capable of blocking ribosome binding at the *tap* translation initiation site in vitro (Malmgren et al., 1996), suggesting the existence of a bulky structure.

In the present work, the conformation of the stable complex formed by CopA and its target, CopT, was studied using chemical and enzymatic probing (Ehresmann et al., 1987). For comparison, the extended kissing complex formed by the truncated antisense RNA CopI and CopT was tested in parallel. Based on extensive probing results, a model of the CopA–CopT complex was built using computer-graphic modeling. The proposed structure presents as its most unique feature an asymmetric cruciform-like structure whose formation requires extensive breakage of intramolecular base pairing in the upper stems and the formation of intermolecular base-pairing interactions. Base-pair inversions in CopA and compensatory mutations in CopT were introduced in different positions of the upper stems to define the boundaries of the newly formed intermolecular helices. The significance of these structural features is further discussed.

RESULTS

Enzymatic and chemical probing of the antisense and target RNAs

We showed previously that full CopA–CopT duplexes are only slowly formed in vitro, and identified a stable complex using double-strand-specific enzyme RNase III- and Pb^{2+}-catalyzed cleavages (Malmgren et al., 1997). To obtain detailed structural information about the CopA–CopT complex, we used a range of enzymes and chemical reagents. To study the extended kissing complex, CopA was replaced by the truncated CopA variant CopI, which contains only the major stem-loop structure (Persson et al., 1990a). Antisense or target RNAs were end labeled and incubated with complementary, unlabeled counterparts for complex formation under native conditions (see Materials and Methods). RNAs, free or complexed, were subjected to enzyme hydrolysis or chemical modifications under conditions where statistically less than one cleavage/modification per molecule takes place. Enzymes used were RNase T1 (specific for single-stranded guanines), RNase T2 (specific for single-stranded regions), and RNase V1 (specific for double-stranded regions). Dimethylsulfate (DMS; alkylates [N3]C and [N7]G), diethylpyrocarbonate (DEPC; modifies [N7]A), nickel complex (NiCR; modifies [N7]G), and hydroxyl radicals (cleavage at ribose moieties) were used as chemicals. Hydroxyl radicals were only used on end-labeled CopA free or bound to CopT. NiCR (Chen et al., 1993) and DEPC (Weeks & Crothers, 1993) are known to be very sensitive to stacking of base rings. Therefore, position N7 of purines within a helix is not reactive unless the deep groove is widened. RNAs were also subjected to Pb^{2+}-induced cleavage, which has proven exquisitely sensitive to subtle structural variations (Malmgren et al., 1997). Experiments are shown in Figures 2–5, and the determined reactivities are indicated schematically in Figure 6. For convenience, analogous nucleotides in CopA and CopI are referred to by their positions in CopA.

In general, most cleavages/modifications of the free RNAs correlate well with the proposed secondary structures of both RNAs (Fig. 6). The main cleavages by RNases T1 and T2 were located in the external loops and the single-stranded regions, whereas RNase V1 cleavages were only observed in helical regions of both RNAs (Figs. 2 and 4). All cytosines reactive towards DMS were located in loops and single-stranded regions of both RNAs (Fig. 3). The results indicated the existence of a particular structure for loop II of CopT: the absence of a RNase T1 cut at G114 (Fig. 4) and the absence of reactivity at N3 of U109 and N1 of G114 towards chemical probes (Malmgren et al., 1996) were indicative of a U–G base pair closing the loop. This base pair has recently been proposed to occur in a similar loop of *repZ* mRNA (ColIb-P9 plasmid; Asano et al., 1998).

Structure probing of the extended kissing CopI–CopT complex

Binding of CopI induces several reactivity changes in CopT, specifically in loop II′ and the upper stem II′ (Figs. 4 and 6B). Unexpectedly, the major RNase T1 cleavages at G111 and G112 were only weakly decreased (Fig. 4). The RNase T2 cleavages in loop II′ were still observed in the extended kissing complex, whereas significant protection of the weak cleavages occurred at C104, A105, and A118. Upon RNase V1 digestion, new cleavages appeared at C104 and A105, and A106 and C107 became protected (Fig. 4). CopI also induced strong protections at positions [N7]A118 and [N3]C119, and moderate protections at [N3]C101, [N3]C113, [N7]A105, and [N7]A106 (Fig. 6B). These data are in good agreement with the Pb^{2+}-induced cleavages, because strong CopI binding-induced protections were previously observed on both sides of the upper stem II′ of CopT (U102–C107 and U117–A123; Malmgren et al., 1997). In contrast, the entire region of complementarity was rendered resistant to single-strand-specific RNases when full duplexes were formed artificially (Fig. 4).

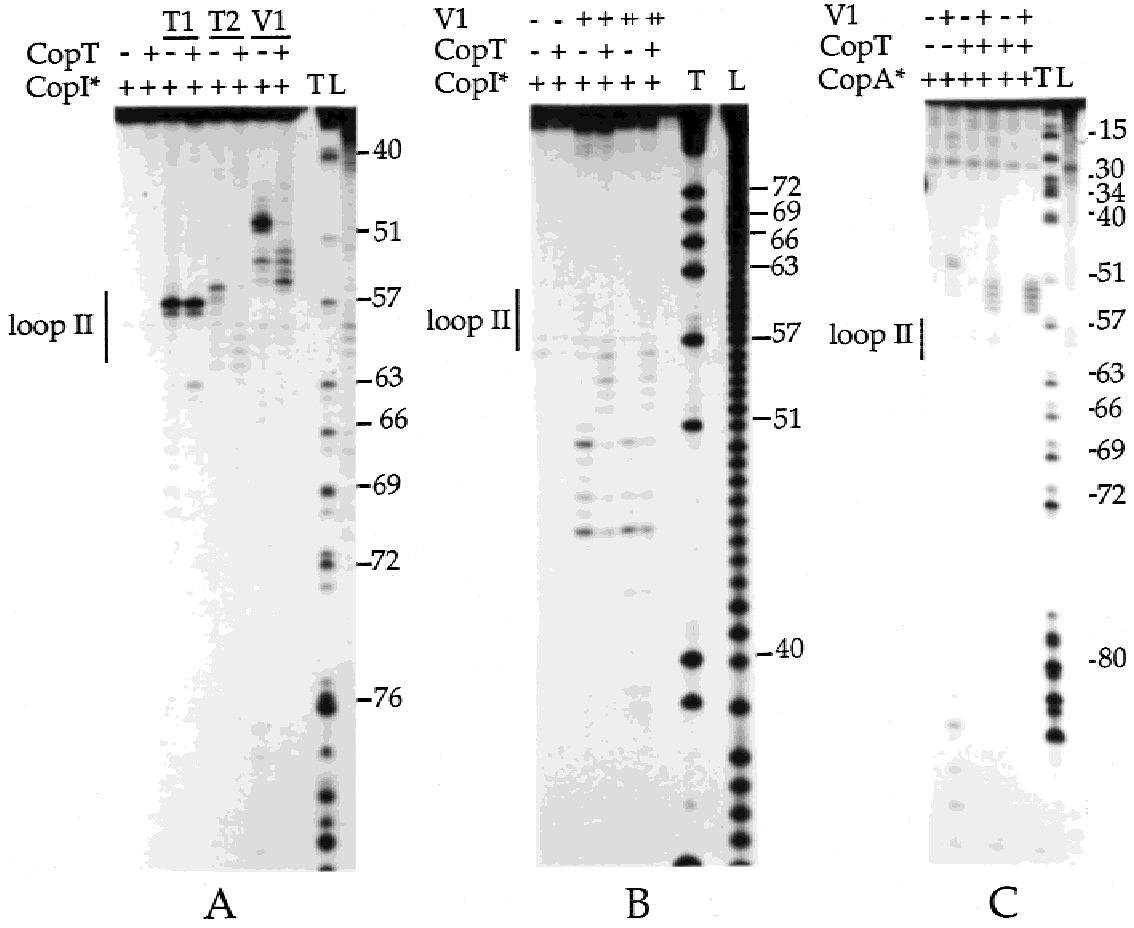

FIGURE 2. Enzymatic hydrolysis of CopI and CopA free or in complex with CopT. Enzymatic hydrolysis on 3′- (**A**) or 5′- (**B**) end-labeled CopI (CopI*), and (**C**) on 3′-end-labeled CopA (CopA*), free (− CopT) or in the presence of an excess of CopT (+ CopT). Complex formation was performed at 37 °C for 5 min. Enzymatic reactions were done at 37 °C for 5 min. T1: RNase T1, 0.001 unit; T2: RNase T2, 0.01 unit; V1: RNase V1, 0.05 (+) or 0.1 (++) U. Lanes T, L: RNase T1 and alkaline ladders, respectively.

Binding of CopT induced similarly located reactivity changes in loop II and the upper stem II of CopI (Figs. 2 and 3). The major RNase T1 cut at G57 remained unchanged or was only weakly protected, and a new weak cut appears at G63 (Fig. 2A). The strong RNase T2 cleavage at C56 became protected upon CopT binding whereas the cleavages at positions 60–62 were slightly enhanced (Fig. 2A). Again, these data were in accordance with the susceptibility of loop II of CopI to Pb^{2+}-catalyzed hydrolysis in the extended kissing complex (Malmgren et al., 1997). CopT also induced significant protection at [N3]C56 whereas cytosines 58–59 remained reactive at N3 (Fig. 3B), and adenines 60–61 at N7. RNase V1 hydrolysis was decreased at positions 48–50, concomitant with the appearance of new cleavages at positions 52–56 (Fig. 2). These new RNase V1 cleavages were not observed in the full CopA–CopT duplexes formed artificially (data not shown).

Thus, the accessibility of nt 57–63 in CopI and 107–113 in CopT to single-strand-specific probes and the RNase V1 cuts at positions 52–56 in CopI and 104–107 in CopT indicate that formation of the extended kissing complex requires intermolecular interactions in the upper stem regions at the expense of intramolecular base pairs.

Structure probing of the stable CopA–CopT complex

CopA–CopT complexes were formed at 37 °C for 2–15 min and subjected to enzymatic cleavages or chemical modifications. We previously showed that within 15 min of incubation, at given concentrations, most RNAs were in the form of stable complexes, but only a minor fraction was converted to a full duplex (Malmgren et al., 1997).

CopA and CopI induced virtually indistinguishable reactivity changes in the stem-loop II′ of CopT (Fig. 6B). In particular, residues in loop II′ remained accessible to the single-strand-specific RNases and Pb^{2+} hydrolysis when CopA–CopT complexes were analyzed (Fig. 4). Furthermore, enhanced RNase V1 cuts also occurred

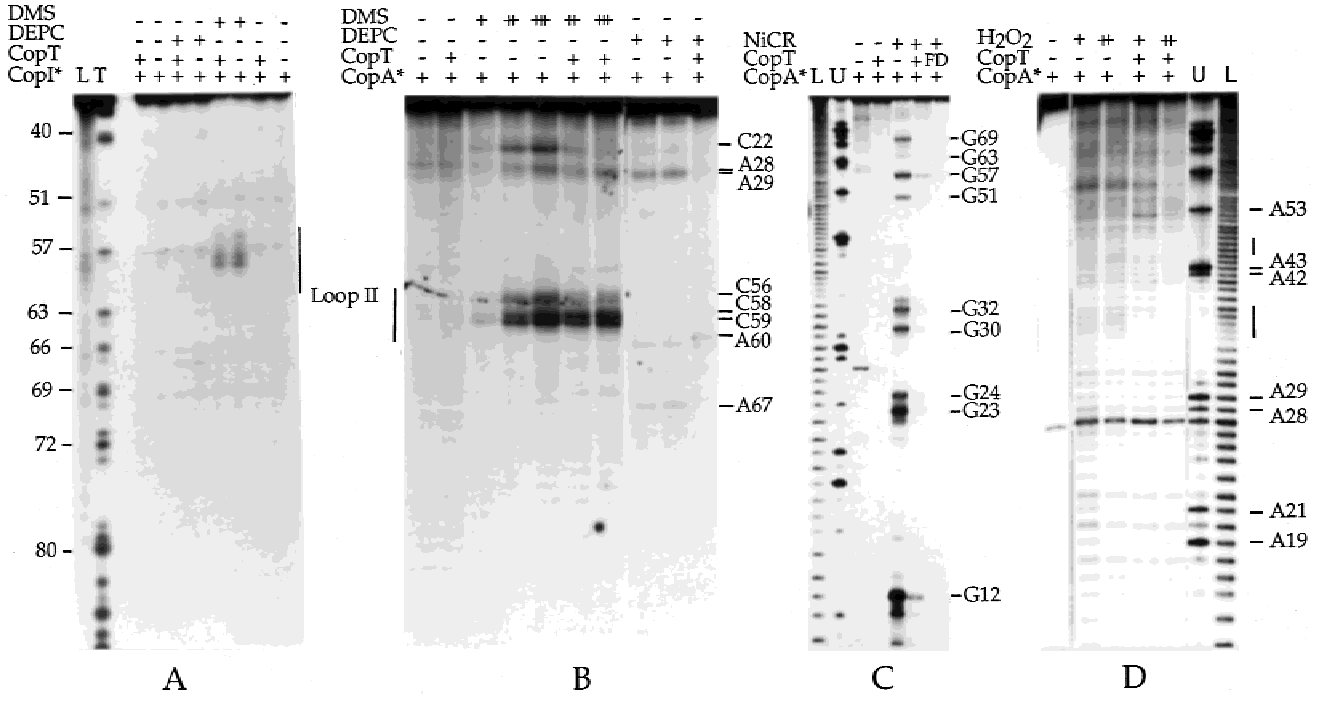

FIGURE 3. Chemical probing of CopA and CopI, free or in complex with CopT. **A**,**B**: DMS (N3C) or DEPC (N7A) modifications on (**A**) 3′-end-labeled CopI (CopI*) or (**B**) CopA (CopA*), free (− CopT) or bound to CopT (+ CopT). Complex formation with CopT was performed at 37 °C for 5 min. DMS, native conditions: 5 min (+), 10 min (++), and 15 min (+++) at 37 °C; DEPC, native conditions: 20 min at 37 °C. (**C**) NiCR modification on 5′-end-labeled CopA: free (− CopT), bound to CopT under native conditions (+ CopT), and full CopA–CopT duplex (FD); (**D**) Hydroxyl radical hydrolysis on 5′-end-labeled CopA free (− CopT) or bound to CopT (+ CopT). Reactions were performed either in the presence of H_2O_2 1% (+) or 10% (++). Lanes L, T, U: Alkaline, RNase T1, and RNase U2 ladders, respectively.

at C104 and A105. Additional strong protections were observed in the 140–169 region (T2, T1, and Pb^{2+} cleavages) and, concomitantly, new RNase V1 cuts appeared at U162–C163 and U167–A168 (Fig. 4). In contrast, formation of a full duplex between CopA and CopT conferred complete protection of the CopA binding site (positions 80–169) from single-strand-specific probes but induced new RNase V1 cuts at U162–C163 and U167–A168 (Fig. 4). In the case of the native complex, no major structural rearrangement of CopT RNA occurred in the noncomplementary region (Fig. 4). Minor changes were represented by enhanced RNase T1 cleavages at G172 and G173 in the Shine–Dalgarno sequence of *tap*, indicating melting of stem I′.

Conversely, CopT induced the same reactivity changes in stem-loop II of CopI and CopA (see Figs. 2 and 3). This is well illustrated by the new RNase V1 cuts at positions U52–C56 and the accessibility of residues 57–61 towards chemicals and RNase T2 (Figs. 2 and 3). Furthermore, most of the N7 position of guanines, with the exception of G57, showed protection towards NiCR (Fig. 3C). In addition, strong protections were detected in the 5′ tail of CopA encompassing nt 1–30 (T2 and T1), and [N3]C22 and [N7]/(A9, G23, G24, A28, and A29) were rendered unreactive in the complex (Figs. 2 and 3B). Finally, significant protections were induced by CopT binding at several riboses of CopA, at positions 35–38 and 46–48 (Fig. 3D).

These results further confirm that a full duplex between CopA and CopT is not rapidly formed in vitro. Instead, the extended intermolecular interactions present in the CopI–CopT complex are maintained in the CopA–CopT complex. These data suggest the formation of two intermolecular helices, B and B′, thus generating a four-helix junction. Additionally, the extended kissing complex is stabilized by an intermolecular helix C formed between the 5′ most 30 nt of CopA and the complementary sequences of CopT.

Base-pair inversions in stems II/II′ of CopA and CopT alter the formation of helices B and B′

Structure mapping of the complexes formed by CopI–CopT and CopA–CopT supported the presence of two intermolecular helices, B and B′, as modules in the four-helix junction structure (Fig. 6). To delimitate the number of base pairs in the two intermolecular helices, we used site-directed mutagenesis of the *copA/copT* gene sequence. Base-pair inversions were introduced at three positions within stem II. These mutations affect neither the stability nor the structure of the RNAs in their free state (data not shown), but were expected to affect formation of helices B and B′ (Fig. 6). Polymerase chain reaction (PCR)-generated templates were used for transcription of mutated CopI, CopA, and CopT

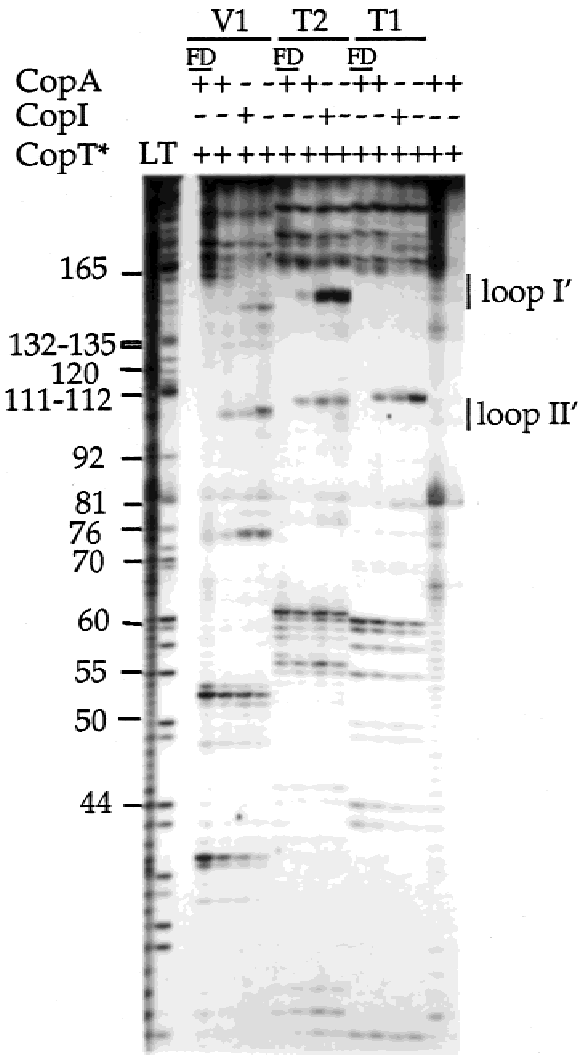

FIGURE 4. Enzymatic probing on CopT, free or in complex with antisense RNAs. Enzymatic hydrolysis on 5′-end-labeled CopT (CopT*). Complex formation with CopI (+ CopI), or with CopA (+ CopA) was performed at 37 °C for 5 min under native conditions. Full duplex with CopA (FD) was formed by denaturation/annealing treatment. Enzymatic hydrolysis were performed with RNase T1, 0.001 U (T1); RNase T2, 0.01 U (T2); RNase V1, 0.1 U (V1).

RNAs. The effect of the mutations on the structure of homologous or heterologous wild-type and mutant CopI–CopT or CopA–CopT pairs were analyzed by enzymatic mapping. Autoradiograms of such experiments are shown in Figure 5.

Cleavages by RNase V1 was used to obtain a signature of the extended kissing complex: new or enhanced cleavages were induced in CopA or CopI at consecutive positions U52–C56, and in CopT at C104–A105. Furthermore, in the CopA–CopT complex, the formation of the intermolecular helix C that greatly enhances complex stability was characterized by several V1 cuts in CopT at U162–C163 and U167–A168, as well as by the disappearance of V1 cleavages in CopA at positions G7–A9 and G16–A19, resulting from melting of helix I. Therefore, we used RNase V1 to probe the structure of the homologous and heterologous complexes formed with the H1, H2, and H3 RNA variants (Fig. 5). In all these experiments, we used conditions (RNA concentrations, time of incubation, buffers) under which the stable CopA–CopT complex is almost quantitatively formed.

RNase V1 probing of end-labeled CopA RNA variants indicated almost identical cleavage patterns of free mutant and wild-type RNAs. Hence, no major structural changes were caused by the mutations. The three homologous CopA/CopT and the heterologous CopA-H3/CopT-wt complexes showed the characteristic RNase V1 patterns, that is, the appearance of cleavages at positions U52–C56 in CopA (Fig. 5A). Interestingly, the heterologous complexes formed between CopT-wt and either CopA-H1 or CopA-H2 were different: significant protections were observed at U49–C50 of CopA-H1 and CopA-H2 (Fig. 5A), whereas positions U52–C56 remained uncleaved, that is, a pattern resembling that of free RNAs. The same experiments were also performed using end-labeled CopT variants (Fig. 5B). Again, no major structural changes occurred in CopT mutant RNAs, and identical cleavage patterns were observed for all homologous CopA–CopT complexes, as well as in the heterologous CopA-wt/CopT-H3 complex. Cleavages at positions C104–A105 in the different CopT species were enhanced after complex formation, and protections occurred at A106–C107 (Fig. 5B). In contrast, CopA-wt/CopT-H1 and CopA-wt/CopT-H2 complexes were not susceptible to cleavage at these positions (Fig. 5B). Identical data were obtained by using the mutated CopI RNAs which cannot form helix C (data not shown).

Thus, the base-pair inversions located above the lower bulge in CopA or CopT (H1 and H2) affected the overall topology of the four-way junction structure, whereas a wild-type-like cleavage pattern was restored by forming complexes between fully complementary RNAs. This supports the presence of canonical intermolecular base pairs in helices B and B′ that are required for RNase V1 hydrolysis in these two regions. In contrast, base-pair inversions below the lower bulged residues (H3) in each of the RNAs did not affect the global structure of the CopA–CopT complex, demonstrating that the corresponding nucleotides are not involved in intermolecular base pairing between CopA and CopT.

A three-dimensional model for the antisense RNA–target RNA complex

A secondary structure model consistent with the probing data is proposed for the CopA–CopT complex and shown in Figure 6C. The intramolecular and intermolecular helices are entirely formed by Watson–Crick base pairs. Our data argue for the formation of two intermolecular helices (B and B′) connected by single-

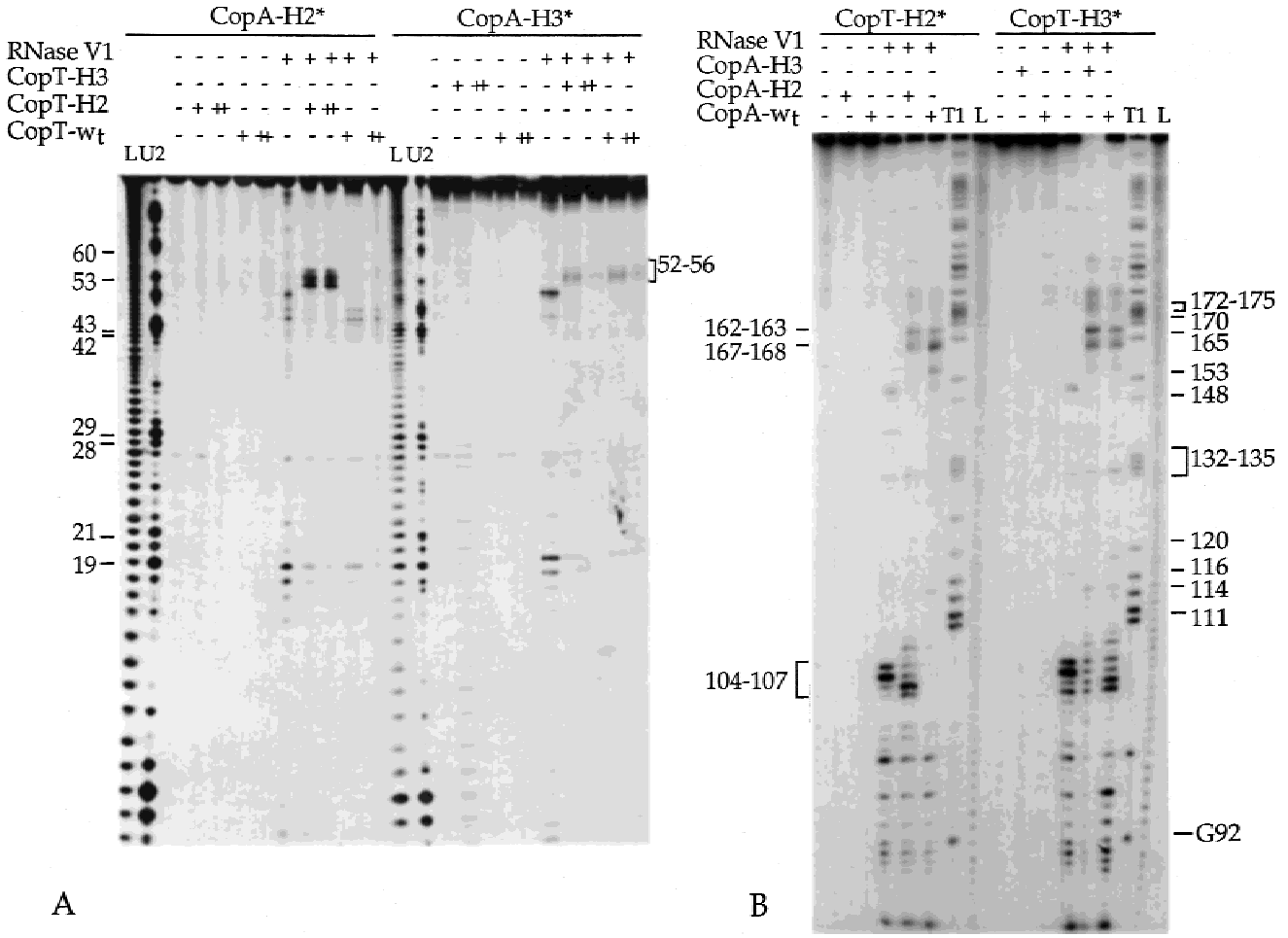

FIGURE 5. RNase V1 probing of homologous or heterologous CopA–CopT complexes. Enzymatic hydrolysis was performed on 5′-end-labeled CopA-H2 or CopA-H3, alone or in the presence of an excess of wild-type or mutant CopT (**A**) and on 5′-end-labeled CopT-H2, or CopT-H3, free or bound to either wild-type or mutant CopA (**B**). Complex formation was performed at 37 °C for 15 min in TMN buffer. Lanes T1, U2, L: RNases T1, U2, and alkaline ladders, respectively.

stranded regions (G57–A62 in CopA, U108–C113 in CopT). These two connecting regions were accessible to single-strand-specific probes (Fig. 6). Helix B contains 9 bp formed between U48–C56 of CopA and G114–A122 of CopT. This is supported by the fact that [N3]C56 and [N7]G51 in CopA, as well as [N3]C119 in CopT, were rendered unreactive, and by the presence of several RNase V1 cuts in CopA. Helix B′ is proposed to consist of 6 bp (G63–A68 in CopA, U102–C107 in CopT), and is supported by several RNase V1 cleavages in CopT and by the unreactivity of guanines 63, 66, and 69 at their N7 position towards NiCR. The number of base pairs in helices B and B′ was also determined by site-directed mutagenesis. Indeed, only base-pair inversions located above the lower bulge in CopA or CopT (H1 and H2) affected the formation of both intermolecular helices. Probing data also showed that the intramolecular helices A′ (35–47/70–83) in CopA and A (88–100/123–135) in CopT remain unchanged in the complex.

As base stacking is a major factor in the stabilization of RNA structures, the four (two intra- and two intermolecular) helices are proposed to stack forming two quasicolinear duplexes, centered around a four-helix junction, as a result of strand exchange between the two complementary RNAs (Fig. 6C). In principle, two types of junctions were possible, as the two helical domains, generated by coaxial stacking, could be constituted by either B–A and B′–A′ (junction 1 in Fig. 6C) or by B′–A and B–A′ (junction 2, not shown). The choice between the two junctions was made with the help of molecular modeling. A three-dimensional model of the CopA–CopT complex was assembled based on the experimental data and stereochemical constraints. Using this approach, the configuration of junction 2 could be rejected due to topological constraints that prevented connection of helices B and B′ via the single-stranded regions. The overall form of the resulting model shown in Figure 6 is that of an asymmetrical cruciform structure. The helical arms stack in pairs (A–B and A′–B′) to generate quasicontinuous, coaxial helices. These two helical domains were slightly rotated to adopt an asymmetrical X-shape required for the accommodation of single-stranded residues in grooves (Fig. 7A,B). This

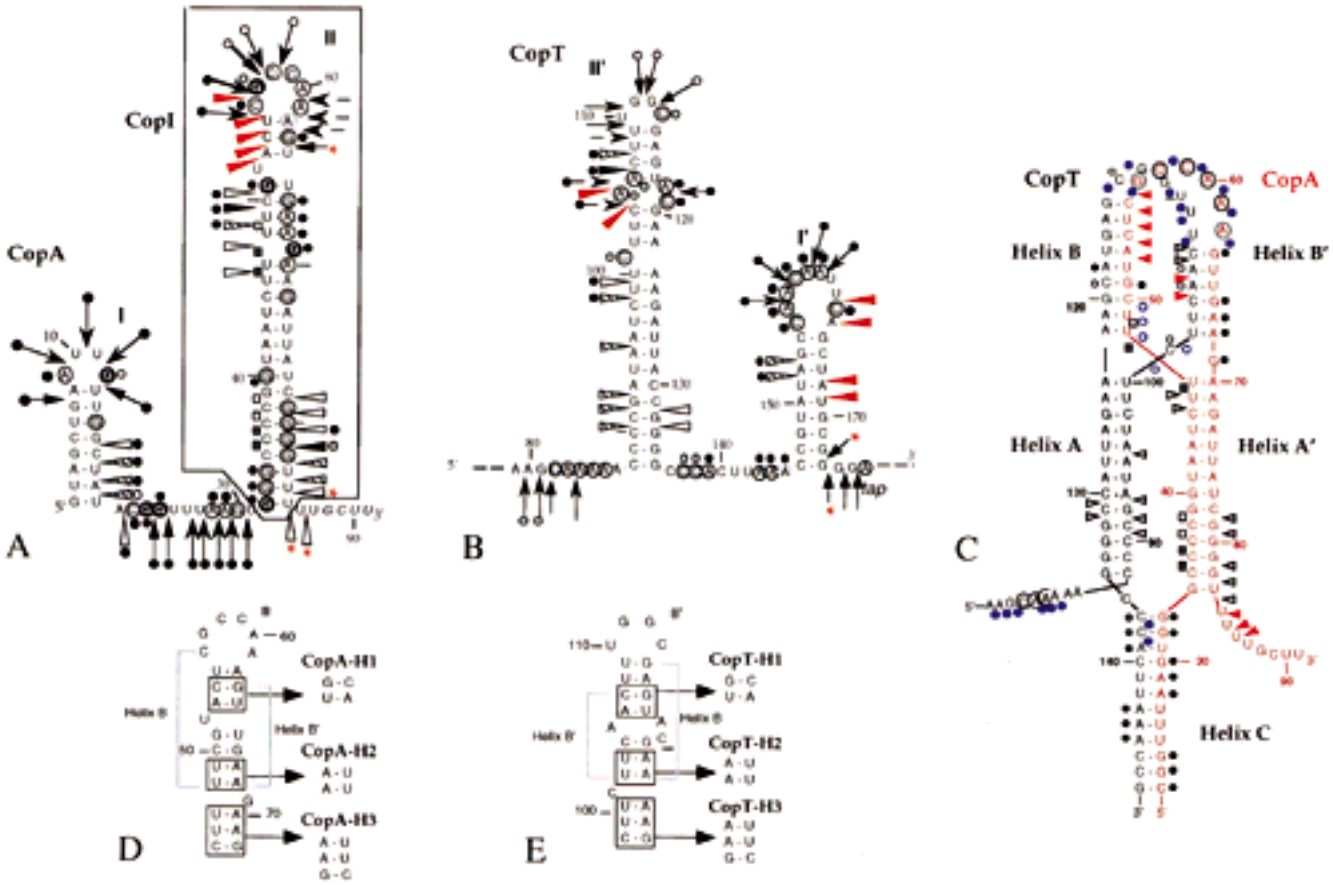

FIGURE 6. Enzymatic and chemical probing on free and complexed RNAs. A summary of the probing results is represented on the secondary structure of CopA (**A**), and CopT (**B**). The sequence of CopI is framed. The reactivity changes in CopI and CopA induced by CopT binding are strictly identical. **A**: Enzymatic cleavages: RNase T1 (o⟶) T2 (o⟶), RNase V1: (◅) low, (◅) moderate, (◅) strong. Chemical modifications: cytosines at position N3, adenines at position N7, and guanines at position N7 reactive under native conditions are circled. The reactivity changes in CopA and CopT in the complex are indicated as follows: strong (filled circle), moderate (grey circle), and weak (open circle) protection; enhancements are represented by asterisks proportional to the intensity. New RNase V1 cleavages are shown by red arrows. Protected riboses in CopA are shown by squares. **C**: Summary of the enzymatic and chemical probing on the secondary structure model of the CopA–CopT complex. Pb^{2+}-cleavages are denoted by blue dots. Circled nucleotides: [N3]C, [N7]A reactive under native conditions. Positions ([N3]C, [N7]A, [N7]G) that became protected in the complex are denoted by black dots. RNase V1 cuts and protected riboses are indicated as described above. RNase T1 and T2 cleavages are not shown. Helix C comprises residues 1–33 of CopA and 137–169 of CopT. Nucleotides of CopA are in red. **D**,**E**: Localization of the mutated nucleotides (H1, H2, and H3) squared on the secondary structure model of CopA (**D**) and CopT (**E**). Nucleotides involved in the intermolecular helices B and B′ are indicated by bars.

was necessary to avoid steric interference between backbones and to permit the connections of B with A′ and B′ with A (Fig. 7C). The transition between crossed helices was accomplished by sharp turns of the backbone between U47 and U48 in CopA and U100 and C101 in CopT. It was difficult to build a canonical base pair between C101 in CopT and G69 in CopA. However, C101 and G69 were stacked within the helix, as their N3 and N7 positions, respectively, were unreactive in the complex (Fig. 6). The two connecting loops (residues 56–62 in CopA and 108–113 in CopT) were accessible to the solvent. Because of the limited number of constraints, a significant variation in local geometry for both loops may occur. Nevertheless, all the topological constraints resulting from the four-way junction are included in the molecular modeling. The unusual folding of the extended kissing complex favors a side-by-side alignment of stems A′ in CopA and A in CopT that facilitates formation of a third intermolecular helix between the 5′-most 30 nt of CopA and the complementary region of CopT (Fig. 7A,B). The close proximity of the phosphate backbone at this resulting three-way junction may explain the protections of several riboses from hydroxyl radicals, observed at position 35–38 in CopA (helix C, Figs. 3C and 6).

A putative divalent metal ion binding site in the CopA–CopT complex

The four-way junction imposes a close proximity of the helices that is well suited for divalent metal-ion binding. Computer modeling based on Brownian-dynamics sim-

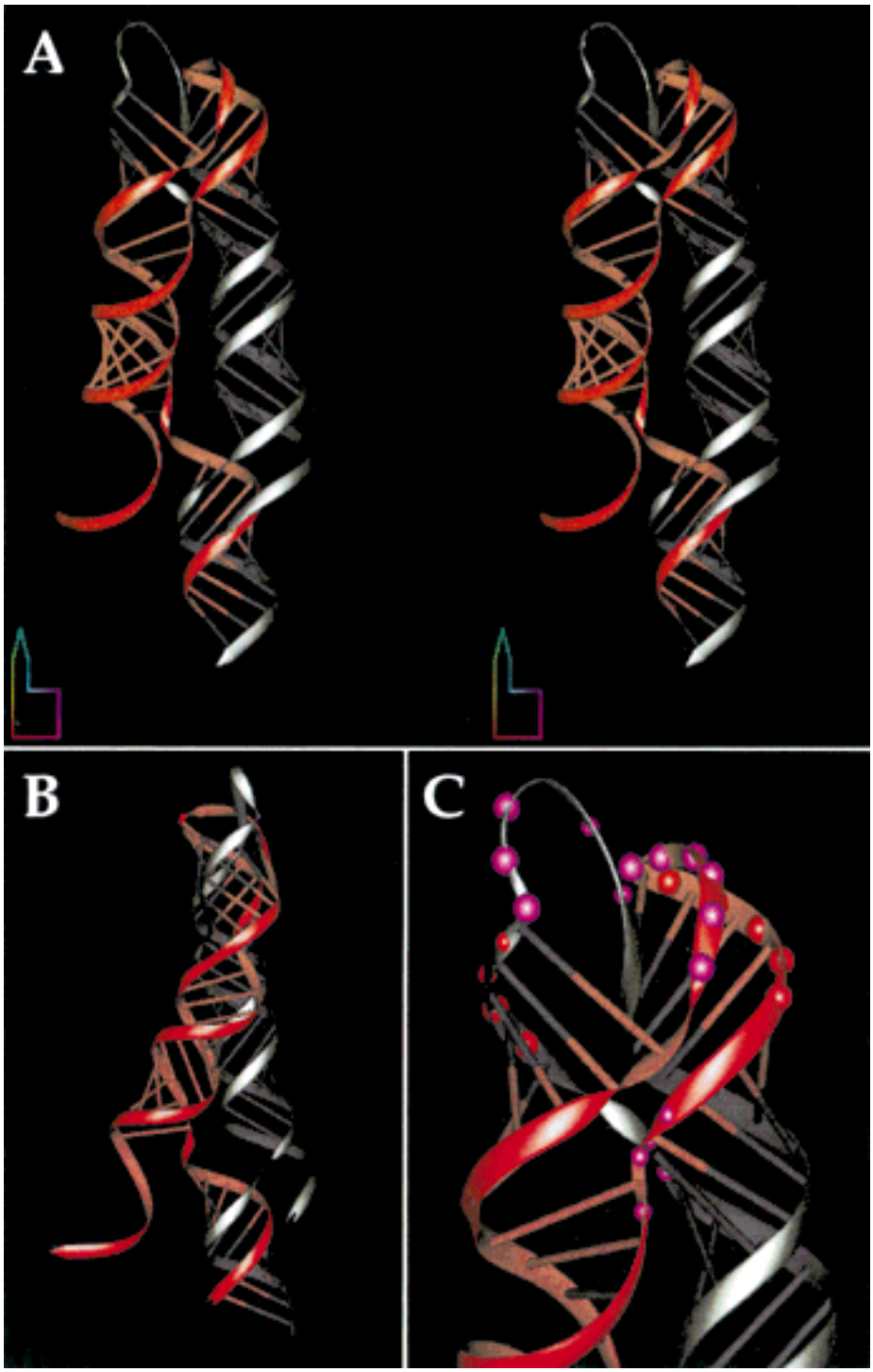

FIGURE 7. Models of the CopA–CopT complex. **A**: Stereoview of the three-dimensional model of the CopA–CopT complex. CopA [20–91] is in red, CopT [80–143] in white. **B**: The complex rotated by 45 degrees. **C**: An enlarged view of the four-way junction. Regions [U102–A122] in CopT and [U48–A68] in CopA are shown. RNase V1 cuts are represented by red dots, and Pb^{2+} cleavages by purple dots. The models were drawn with the program DRAWNA (Massire et al., 1994).

ulations for exploration of metal-ion binding sites in RNAs (Hermann & Westhof, 1998) predicted a magnesium binding site coordinated via the phosphate groups between the two adjacent helical domains (results not shown). With respect to this, the protection of riboses 46–48 towards hydroxyl radicals (Fig. 3D) might be well correlated with the presence of a Mg^{2+} binding pocket, as shown for tRNAs (Latham & Cech, 1989). Strong cleavage induced by Pb^{2+}-catalyzed hydrolysis at precise positions is also indicative of divalent cation

binding sites (for a review, see Pan et al., 1993). Interestingly, the inversion of 2 bp at positions 48–68 and 49–67 in CopA (mutant CopA-H2) and at positions 102–122 and 103–121 in CopT (CopT-H2) causes the appearance of a strong Pb^{2+}-cleavage site at U47 in CopA-H2 or CopI-H2 upon complex formation with CopT-H2 (Fig. 8A). These mutations do not affect the binding rate for the formation of the stable complex (data not shown). Also, the structure of the extended kissing complex is very similar to that of the wild-type CopI–CopT complex (Fig. 5), as indicated by a Pb^{2+}-cleavage pattern encompassing residues U52–G69 of CopI-H2 bound to CopT-H2 that is indistinguishable from that of the wild-type complex: the hairpin loop II of CopI in the complex was still cleaved at C59, A60, A61, and A62, and significant protections occurred on both sides of the upper helix II (Fig. 8B; Malmgren et al., 1997). Cleavage at U47 requires intermolecular base pairing between A48/A49 of the antisense RNA and U121/U122 of CopT, as no enhanced cleavage at U47 was detected in the heterologous complex CopI-H2/CopT-wt (data not shown). Finally, hydrolysis at U47 was strongly reduced by increasing concentrations of Mg^{2+} (Fig. 8C). Thus, the strong lead cleavage at U47 most likely results both from the presence of a divalent metal-ion binding site and from appropriate stereochemistry and mobility of the cleaved phosphodiester bond.

DISCUSSION

Conversion of a loop–loop interaction to a four-helix junction

Previous kinetic and mutational analyses showed that binding is initiated via a loop–loop interaction between the 5′-CGCC-3′ sequence in the hairpin loop of CopA and the complementary sequence of CopT (Persson et al., 1988, 1990b). However, these initial interactions are transient, as the present study of CopA–CopT and CopI–CopT complexes shows that most of the nucle-

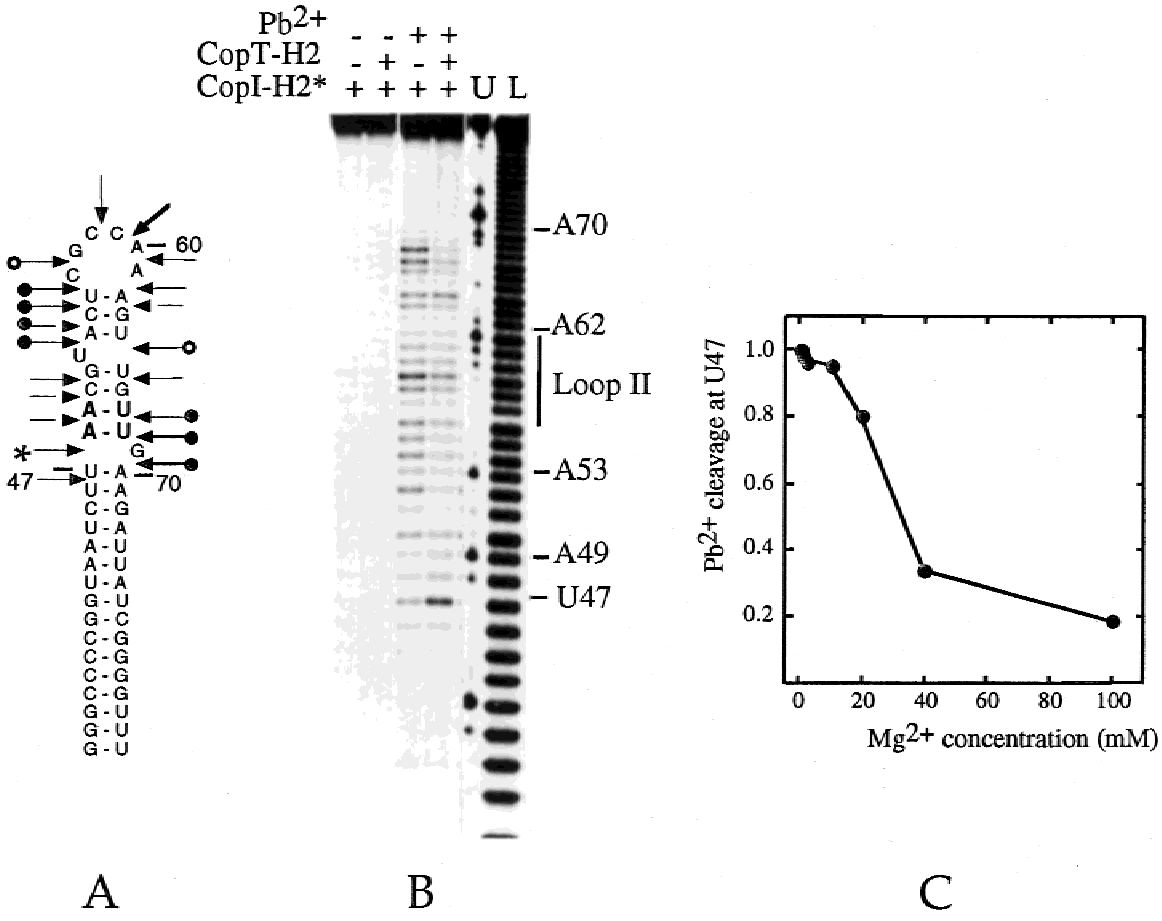

FIGURE 8. Pb(II) probing of CopI-H2 and the effect of binding of CopT-H2. **A**: Secondary structure of CopI-H2 showing the effect of CopT-H2 binding. The mutated nucleotides are shown in bold. Position of Pb^{2+} cleavages in the free RNAs are indicated by arrows. The protections induced by CopT-H2 are shown by spheres, and enhanced cleavage is indicated by an asterisk. **B**: Autoradiogram showing Pb^{2+}-hydrolysis (8 mM) on 5′-end-labeled CopI-H2 alone (− CopT-H2), or in the presence of CopT-H2 (+ CopT-H2). Lanes U, L: RNase U2 and alkaline ladders, respectively. **C**: Effect of magnesium concentration on Pb^{2+} hydrolysis. The intensity of the band corresponding to cleavage at U47 of CopI-H2 complexed to CopT-H2 is depicted as a function of magnesium concentration.

otides in loop II of the antisense RNA, as well as in the complementary target loop, are accessible to single-strand-specific probes. Thus, helix extension from this initial loop–loop complex generates helices B and B′, resulting in disruption of the initiating base pairs and formation of the extended kissing complex (Fig. 6C). The enzymatic and chemical probing data indicate that nucleotides on both sides of the upper stem II segments (48–56, 63–68) of CopA and CopI interact by interstrand pairing with the complementary nucleotides in CopT forming the two intermolecular helices B and B′ (Fig. 6C). Further support comes from the observation that mutations in helices B/B′ that disrupt the complementarity between CopA or CopI and CopT affect the structure of the extended kissing complex. On the other hand, mutations below the lower bulge had no effect on the formation of helices B and B′. Taken together, these results define the boundaries of helices B and B′ (Fig. 6C) and indicate that progression of the intermolecular helices B and B′ is arrested due to topological stress. Consequently, the intramolecular helices A and A′ remain identical in CopI–CopT and CopA–CopT complexes. We infer that conversion of the initial loop–loop interaction to the four-helix junction structure is facilitated by low stability of the upper stem regions, conferred by the bulged residues and the presence of several G–U and A–U base pairs in both RNAs. By independent experiments, it was previously shown that removal of bulges severely impaired binding rates and in vivo control (Hjalt & Wagner, 1995). The results presented here also indicate that complete pairing between CopA and CopT does not occur rapidly in vitro. It is likely that the formation of the peculiar four-helix junction structure results in kinetic or topological entrapment of the complex for extended periods of time (Malmgren et al., 1997; this work).

The extended kissing complex adopts an X-shaped structure with a side-by-side alignment of helical domains

Molecular modeling was used to deduce a global fold of the stable CopA–CopT complex. The validity of the overall architecture presented relies on a variety of experimental data (chemical and enzymatic probing; effect of mutations on CopA–CopT structure) that were used to assemble a structure with appropriate stereochemistry. We propose that the folding of the extended kissing complex at the four-way junction adopts an asymmetric stacked cruciform structure, formed by the colinear helices B–A and B′–A′ in a parallel configuration (Figs. 6C and 7). This model predicts a close contact between helices at the stacked cruciform junction (Fig. 7). Such a negatively charged cavity is likely to bind divalent ions with high affinity. Interestingly, computer modeling based on Brownian-dynamics simulations (Hermann & Westhof, 1998) predicted a magnesium-binding site coordinated via the phosphate groups between the two adjacent helical domains that may explain the protection of riboses 46–48 of CopA bound to CopT towards hydroxyl radicals (Fig. 3D). The presence of a divalent ion at the junction is also suggested by a strong Pb^{2+} cleavage at position 47 of CopA-H2 bound to CopT-H2 that was strongly reduced by increasing concentrations of magnesium (Fig. 8). Finally, we recently observed that magnesium ions are essential for optimal formation of the stable CopA–CopT complex (data not shown).

The overall topology structure of the extended kissing complex is similar to some other RNA four-way junctions (Krol et al., 1990; Walter et al., 1998a; Nowakowski et al., 1999) and DNA Holliday junctions (Duckett et al., 1992). In both DNA and RNA four-way junctions, divalent ions are required for the formation and stabilization of antiparallel X-shaped structures (Duckett et al., 1992; Walter et al., 1998b). The particularity of the proposed CopA–CopT structure is the crossing over of the strands at the junction under the constraints imposed by the two loops connecting intermolecular helices B and B′. This forces a side-by-side alignment of the two helical domains that brings the 5′ tail of CopA in close proximity to the complementary region of CopT (Fig. 7). The formation of intermolecular helix C, which clamps the two long helical domains, greatly enhances the stability of the complex (Persson et al., 1990a; Malmgren et al., 1997). Crystallographic analysis of a group I ribozyme domain revealed a similar organization (Cate et al., 1996): a sharp bend induced by an internal loop allows a side-by-side alignment of two helical domains that is additionally stabilized by metal- and ribose-mediated backbone contacts and two long-range tertiary interactions. A side-by-side configuration was also proposed for the hairpin ribozyme, here stabilized by interactions between two internal loops (Earnshaw et al., 1997).

The formation of a stable RNA–RNA complex is not unique to CopA–CopT, and is also a key feature in the replication control of plasmids belonging to the IncB and Inclα groups (Siemering et al., 1994; Asano & Mizobuchi, 1998; Asano et al., 1998) plasmids. In these systems, the antisense RNAs inhibit the formation of a pseudoknot structure that activates *rep* translation (Wilson et al., 1993; Asano & Mizobuchi, 1998). All these antisense and target RNAs are characterized by stable hairpins with identical loop sequences and bulged residues in the upper stem regions. Enzymatic probing performed on (antisense) RNAI in pMU720 plasmid bound to its target indicated that a full duplex was not rapidly formed in vitro. Instead, binding resulted in an extended kissing complex stabilized by 5′ tail interactions (Siemering et al., 1994). One may therefore speculate that, in all these systems, the final product of the binding reaction in vitro is characterized by an overall topology very similar to that reported here, except

that the lengths of helices B and B′, if formed in the IncB/IncIα cases, could be different.

Functional implications of the CopA–CopT structure for regulation

The role of CopA is to regulate the synthesis of RepA protein. Previous work showed that the stable CopA/CopT complex detected in vitro prevents ribosome from initiation complex formation at the *tap* RBS (Malmgren et al., 1996). CopI, the truncated antisense RNA unable to form fully paired duplexes, also repressed *repA* expression (Wagner et al., 1992), and the extended kissing complex (CopI–CopT) sufficed to transiently interfere with ribosome binding (Malmgren et al., 1996). We show here that the conversion of the loop–loop interaction to the four-helix junction occurs in both CopA–CopT and CopI–CopT complexes (Fig. 7). Therefore, association of the stabilizer segments (Helix C) of both CopA and CopT is not required for the formation of the extended kissing complex. Experiments with mismatched RNAs carrying mutations H1 and H2 indicate that rapid base pairing throughout helices B and B′ is essential for the formation of the stable CopA–CopT complex and in vivo control (F.A. Kolb, H. Engdhal, E.G.H. Wagner, & P. Romby, in prep.). This implicates the formation of helices B and, most likely B′, in promoting the side-by-side alignment required for formation of the stabilizer helix C and, thus, the inhibitory complex. Binding of CopI or CopA does not induce major conformational changes in the noncomplementary sequences of CopT, that is, the *tap* and *repA* RBS regions, in agreement with previous results (Öhman & Wagner, 1989; Malmgren et al., 1997). The model proposed here for the CopI–CopT complex is a bulky structure (Fig. 7) that might, by steric hindrance, prevent ribosome binding at *tap*. In full-length CopA, the presence of its 5′ extension has several functional implications. It stabilizes the extended kissing complex, providing approximately three helical turns of double-stranded RNA immediately 5′ of the *tap* SD. Thus, its main role is to promote complete and irreversible inhibition of *tap* translation. This intermolecular helix is also a substrate for RNase III cleavage, although destabilization of *repA* mRNA contributes little to control of *repA* expression (Blomberg et al., 1990). Finally, factors that alter CopA turnover will also affect plasmid copy number, because the degree of inhibition is correlated with the intracellular concentration of CopA. The 5′ tail of CopA carries a cleavage site for RNase E, the enzyme that initiates rapid turnover of CopA (Söderbom et al., 1997).

In many regulatory antisense systems, the formation of complete antisense-target RNA duplexes appears to be a slow process in vitro and often becomes arrested at the stage of a stable binding intermediate (Wagner & Brantl, 1998; Zeiler & Simons, 1998). For CopA–CopT, topological barriers are encountered during helix propagation, especially at the four-way junction of the extended kissing complex. Coaxial stacking with parallel packing of helices is known to be a general driving force towards RNA folding and probably contributes to the stabilization of the CopA–CopT binding intermediate. Moreover, unwinding of the stems of CopA and CopT from helix C, although topologically possible, requires overcoming important energy barriers. Thus, the CopA–CopT system appears to exploit binding intermediates as active key structures for the inhibitory step, rather than fully paired species.

So far, direct experimental evidence on structures of CopA–CopT complexes in bacterial cells is lacking. However, identically located RNase III-dependent cleavages occurring on both RNAs in vitro and in vivo (Blomberg et al., 1990; Malmgren et al., 1997) provide circumstantial evidence that, even in the cell, binding may be arrested at the stage of the extended kissing complex stabilized by the intermolecular helix C.

MATERIALS AND METHODS

Oligodeoxyribonucleotides

For RNA transcription in vitro, PCR fragments containing mutations H1, H2, or H3 were generated from the pGW177-III-L series plasmids using the following primer pairs: for CopT-H1: 5T-H1(5′ ACG TAC TTT AAA GCA AAA ACC CCG ATA ATC TTC TTC ATG TTT GGC GAC AAC GAA AAG ATT ACC G 3′) and SeqP-BamHI (5′ CGC GGA TCC CGG ATT CGG GTT CTT TA 3′); for CopT-H2: 5T-H2 (5′ ACG TAC TTT AAA GCA AAA ACC CCG ATA ATC TTC AAC AAC TTT GGC GAG TAC GTT AAG ATT ACC GGG GCC 3′) and SeqP-BamHI; for CopT-H3: 5T-H3 (5′ ACG TAC TTT AAA GCA AAA ACC CCG ATA ATG AAC TTC AAC TTT GGC GAG TAC GAA TTC ATT ACC GGG GCC CAC 3′) and SeqP-BamHI. The resulting PCR-fragments were cloned in the vector plasmid pUT7 (Serganov et al., 1997).

DNA templates and RNA synthesis

CopT, CopA, CopI, and the mutant RNAs (H1–H3) were synthesized by T7 RNA polymerase from PCR-generated DNA fragments as described (Hjalt & Wagner, 1992). PCR fragments were generated from plasmid pGW58 (Blomberg et al., 1990) carrying the wild-type *copA*/*copT* region. Transcription of CopT yields a run-off product of 302 nt initiated with GG instead of the GU sequence of the wild-type *repA* mRNA. The CopA RNA contains a 5′ terminal G instead of an A residue. Neither of these nucleotide changes affects structure or binding properties. In CopA or CopI mutants, 2 or 3 bp were inverted as shown in Figure 6. The complementary changes were also introduced in CopT mutants. Purification of RNAs was performed by fast protein liquid chromatography (FPLC, Pharmacia) on a Bio-Sil TSK250 column. The RNAs were eluted by 0.2 M sodium acetate, pH 6.5, containing 1% methanol, and precipitated.

5′-end labeling of dephosphorylated RNA was performed with T4 polynucleotide kinase and [γ-^{32}P]ATP (Maniatis et al.,

1982). 3′-end labeling of RNA was performed with T4 RNA ligase and [^{32}P]-pCp (England & Uhlenbeck, 1978). Labeled RNAs were purified by polyacrylamide-urea gel electrophoresis, eluted, and precipitated twice with ethanol. Before use, the RNAs were dissolved in water and renatured by incubation at 90 °C for 2 min, followed by slow cooling at 20 °C in TMN buffer (20 mM Tris-acetate, pH 7.5, 10 mM Mg-acetate, 100 mM sodium acetate).

Enzymatic probing

Antisense RNA binding was carried out at 37 °C for 1–15 min in TMN buffer with end-labeled CopT (3×10^{-8} M) and a fivefold excess of unlabeled CopA or CopI (1.5×10^{-7} M), or with end-labeled CopA or CopI (4×10^{-8} M) and a fivefold excess of unlabeled CopT (2×10^{-7} M). Full duplexes between CopT and antisense RNA species were formed by incubation at 90 °C for 2 min followed by slow cooling to 37 °C in TMN buffer. Enzymatic hydrolysis was performed in 10 μL of TMN, in the presence of 1 μg carrier tRNA at 37 °C for 5 min: RNase T1 (0.0025 U), RNase V1 (0.1 U), RNase T2 (0.05 U). Reactions were stopped by phenol/chloroform extraction, followed by ethanol precipitation, and washing with 80% ethanol. Incubation controls were done in parallel to detect nicks in the RNA.

Chemical probing

RNA–RNA complex formation was performed as described above. Chemical modifications of end-labeled RNA, free or in complex, were performed at 37 °C in 20 μL of TMN containing 2 μg of carrier tRNA. Alkylations of [N3]C and [N7]G positions were done with 1 μL DMS (diluted 1/8 in ethanol) for 5 and 10 min, and modifications at [N7]A positions were done with 5 μL of DEPC for 20 and 40 min. After ethanol precipitation, cleavage at modified C residues was induced by incubation with 10 μL of 50% hydrazine for 5 min on ice, and cleavage at modified G residues was performed in 10 μL of 1 M Tris-HCl, pH 8.3, and 10 μL of sodium borohydride (8 mg/mL) for 10 min on ice. All samples were then treated by aniline (Peattie & Gilbert, 1980). Reactions were stopped by ethanol precipitation in the presence of 0.3 M sodium acetate pH 6.0. RNA pellets were washed twice in 80% ethanol and vacuum dried.

Pb^{2+}-induced hydrolysis was done in 20 mM HEPES-NaOH, pH 7.5, 10 mM Mg-acetate, 100 mM sodium acetate, in the presence of 8 or 16 mM $PbOAc_2$ for 5 min. Reactions were stopped by addition of 50 mM EDTA, followed by ethanol precipitation and treatment as above.

Modification of [N7]G by NiCR was performed according to Chen et al. (1993) in 20 μL containing 25 mM phosphate-KOH, pH 7.0, 10 mM $MgCl_2$, 100 mM NaCl, 2 μg carrier tRNA, in the presence of 3 μM NiCR and 200 μM $KHSO_5$. Incubation was for 30 min at 20 °C. Reactions were quenched by addition of 180 μL of a solution containing 3 μg of carrier tRNA, 0.3 M NaOAc, 10 mM Tris-HCl, pH 7.5, 10 mM EDTA, and 0.5% (w/v) sodium dodecyl sulphate (SDS), followed by ethanol precipitation. Cleavages at modified G residues were induced by aniline treatment (Peattie & Gilbert, 1980). Reactions were stopped by ethanol precipitation and treated as above.

Fe(II)-EDTA reactions were done in 25 μL of TMN buffer in the presence of 1 μg carrier tRNA, 2 mM $Fe(SO_4)_2(NH_4)_2$, 4 mM EDTA, 1 mM DTE, 0.1% H_2O_2 for 10 min on ice. Reactions were stopped by ethanol precipitation and treated as above.

Identification of cleavage sites

End-labeled RNA fragments were dissolved in loading buffer (formamide 93%, 30 mM EDTA, xylene cyanol 0.05%, bromophenol blue 0.05%, SDS 0.5%), incubated at 90 °C for 3 min, and sized on 15% polyacrylamide/8 M urea gels. Cleavage positions were identified by running in parallel RNase T1, RNase U2, and alkaline ladders of the end-labeled RNA (Donis-Keller et al., 1977). Incubation controls were done to detect nicks in the RNA.

Graphic modeling

The three-dimensional model of CopT (nt A85–A150) interacting with CopA (nt U20–U91) was built using several algorithms (Westhof, 1993) incorporated in the program MANIP (Massire & Westhof, 1998). The generated model was subjected to restrained least-squares refinement using the programs NUCLIN and NUCLSQ (Westhof, 1993) to ensure geometry and stereochemistry with allowed distances between interacting atoms and to avoid steric conflicts. The color views were generated with the program DRAWNA (Massire et al., 1994). The model was then tested by comparing the theoretical accessibility of atoms with the observed experimental reactivities, as described earlier (Westhof et al., 1989).

ACKNOWLEDGMENTS

We thank Drs. B. Masquida and C. Massire for their help during graphic modeling and helpful discussions, S. Lodmell for stimulating discussions and critical reading of the manuscript, and T. Hermann for the exploration of metal-ion binding sites. We are also grateful to Dr. S. Rokita for providing us with the NiCR compound. C.M. was supported by a fellowship from the Swedish Institute. This work was supported by grants from Centre National de la Recherche Scientifique (CNRS), Ministère des affaires étrangères (MAE) through a PICS (Programme International de Coopération Scientifique, P.R.), and by the Swedish Natural Science Research Council (NFR, G.W.) and Swedish Research Council for Engineering Sciences (TFR, G.W.).

Received September 29, 1999; returned for revision November 15, 1999; revised manuscript received November 24, 1999

REFERENCES

Asano K, Mizobuchi K. 1998. An RNA pseudoknot as the molecular switch for translation of the *repZ* gene encoding the replication initiator of the Inclα plasmid ColIb-P9. *J Biol Chem 273*:11815–11825.

Asano K, Niimi T, Yokoyama S, Mizobuchi K. 1998. Structural basis for binding of the plasmid ColIb-P9 antisense Inc RNA to its target RNA with the 5′-rUUGGCG-3′ motif in the loop sequence. *J Biol Chem 273*:11826–11838.

Blomberg P, Engdahl HM, Malmgren C, Romby P, Wagner EGH. 1994. Replication control of plasmid R1: Disruption of an inhibitory RNA structure that sequesters the *repA* ribosome binding site permits *tap*-independent RepA synthesis. *Mol Microbiol 12*: 49–60.

Blomberg P, Nordström K, Wagner EGH. 1992. Replication control of plasmid R1: RepA synthesis is regulated by CopA RNA through inhibition of leader peptide translation. *EMBO J 11*:2675–2683.

Blomberg P, Wagner EGH, Nordström K. 1990. Control of replication of plasmid R1: The duplex between the antisense RNA, CopA, and its target, CopT, is processed specifically in vivo and in vitro by RNase III. *EMBO J 9*:2331–2340.

Cate JH, Gooding AR, Podell E, Zhou K, Golden BL, Kundrot GE, Cech TR, Doudna J. 1996. Crystal structure of a group 1 ribozyme domain: Principles of RNA packing. *Science 273*:1678–1685.

Chen X, Woodson SA, Burrows CJ, Rokita SE. 1993. A highly sensitive probe for guanine N7 in folded structures of RNA: Application to tRNA-Phe and *Tetrahymena* group I intron. *Biochemistry* 32:7610–7616.

Donis-Keller H, Maxam AM, Gilbert W. 1977. Mapping adenines, guanines, and pyrimidines in RNA. *Nucleic Acids Res 4*:2527–2538.

Duckett DR, Murchie AIH, Bhattacharyya A, Clegg RM, Diekmann S, Kitzing E, Lilley DMJ. 1992. The structure of DNA junctions and their interaction with enzymes. *Eur J Biochem 207*:285–295.

Earnshaw DJ, Masquida B, Müller S, Sigurdsson STh, Eckstein F, Westhof E, Gait M. 1997 Inter-domain cross-linking and molecular modeling of the hairpin ribozyme. *J Mol Biol 274*:197–212.

Eguchi Y, Itoh T, Tomizawa J. 1991. Antisense RNA. *Annu Rev Biochem* 60:631–652.

Eguchi Y, Tomizawa J. 1991. Complexes formed by complementary RNA stem-loops. Their formations, structures and interactions with ColE1 Rom protein. *J Mol Biol 220*:831–842.

Ehresmann C, Baudin F, Mougel M, Romby P, Ebel JP, Ehresmann B. 1987. Probing the structure of RNAs in solution. *Nucleic Acids Res 16*:9109–9128.

England TE, Uhlenbeck OC. 1978. 3′-terminal labeling of RNA with T4 RNA ligase. *Nature 275*:560–561.

Hermann T, Westhof E. 1998. Exploration of metal ion binding sites in RNA folds by Brownian-dynamics simulations. *Structure 15*: 1303–1314.

Hjalt T, Wagner EGH. 1992. The effect of loop size in antisense and target RNAs on the efficiency of antisense RNA control. *Nucleic Acids Res 20*:6723–6732.

Hjalt T, Wagner EGH. 1995. Bulged-out nucleotides in an antisense RNA are required for rapid target RNA binding in vitro and inhibition in vivo. *Nucleic Acids Res 23*:571–579.

Kittle JD, Simons RW, Lee Y, Kleckner N. 1989. Insertion sequence *IS*10 antisense pairing initiates by an interaction between the 5′ end of the target RNA and a loop in the antisense RNA. *J Mol Biol 210*:561–572.

Krol A, Westhof E, Bach M, Lührmann R, Ebel JP, Carbon P. 1990. Solution structure of human U1 snRNA: Derivation of a possible three-dimensional model. *Nucleic Acids Res 18*:3803–3811.

Latham JA, Cech TR. 1989. Defining the inside and outside of a catalytic RNA molecule. *Science 245*:276–282.

Lee AJ, Crothers DM. 1998. The solution structure of an RNA loop–loop complex: The ColE1 inverted loop sequence. *Structure 6*:993–1005.

Malmgren C, Engdahl H, Romby P, Wagner EGH. 1996. An antisense/target RNA duplex or a strong intramolecular RNA structure 5′ of a translation initiation signal blocks ribosome binding: The case of plasmid R1. *RNA 2*:1022–1032.

Malmgren C, Wagner EGH, Ehresmann C, Ehresmann B, Romby P. 1997. Antisense RNA control of plasmid R1 replication: The dominant product of the antisense RNA–mRNA binding is not a full RNA duplex. *J Biol Chem 19*:12508–12512.

Maniatis T, Fritsch EF, Sambrook J. 1982. *Molecular cloning: A laboratory manual*. Cold Spring Harbor, New York: Cold Spring Harbor Laboratory Press.

Marino JP, Gregorian RS, Csankovski G, Crothers DM. 1995. Bent helix formation between RNA hairpins with complementary loops. *Science 268*:1448–1454.

Massire C, Gaspin C, Westhof E. 1994. A program for drawing schematic views of nucleic acids. *J Mol Graph 12*:201–206.

Massire C, Westhof E. 1998. MANIP: An interactive tool for the modeling of ribonucleic acids. *J Mol Graph 16*:197–205.

Nowakowski J, Shim PJ, Prasad GS, Stout CD, Joyce GF 1999. Crystal structure of an 82-nucleotide RNA-DNA complex formed by the 10–23 DNA enzyme. *Nat Struct Biol 6*:151–156.

Öhman M, Wagner EGH. 1989. Secondary structure analysis of the RepA mRNA leader transcript involved in control of plasmid R1. *Nucleic Acids Res 17*:2557–2579.

Pan T, Long DM, Uhlenbeck OC. 1993. Divalent metal ions in RNA folding and catalysis. In: Gesteland RF, Atkins JF, eds. *The RNA world*. Cold Spring Harbor, New York: Cold Spring Harbor Laboratory Press. pp 271–302.

Peattie DA, Gilbert W. 1980. Chemical probes for higher-order structure in RNA. *Proc Natl Acad Sci USA 77*:4679–4682.

Persson C, Wagner EGH, Nordström K. 1988. Control of replication of plasmid R1: Kinetics of in vitro interaction between the antisense RNA, CopA, and its target, CopT. *EMBO J 7*:3279–3288.

Persson C, Wagner EGH, Nordström K. 1990a. Control of replication of plasmid R1: Structures and sequences of the antisense RNA, CopA, required for its binding to the target RNA, CopT. *EMBO J 9*:3767–3775.

Persson C, Wagner EGH, Nordström K. 1990b. Control of replication of plasmid R1: Formation of an initial transient complex is rate-limiting for antisense RNA-target RNA pairing. *EMBO J 9*:3777–3785.

Serganov A, Rak A, Garber M, Reinbolt J, Ehresmann B, Ehresmann C, Grunberg-Manago M, Portier C. 1997. Ribosomal protein S15 from *Thermus thermophilus*: Cloning, sequencing, overexpression of the gene and RNA-binding properties of the protein. *Eur J Biochem 246*:291–300.

Siemering KR, Praszkier J, Pittard AJ. 1994. Mechanism of binding of the antisense and target RNAs involved in the regulation of IncB plasmid replication. *J Bacteriol 176*:2677–2688.

Söderbom F, Binnie U, Masters M, Wagner EGH. 1997. Regulation of plasmid R1 replication: PcnB and RNase E expedite the decay of the antisense RNA, CopA. *Mol Microbiol 26*:493–504.

Thisted T, Sørensen NS, Wagner EGH, Gerdes K. 1994. Mechanism of post-segregational killing: Sok antisense RNA interacts with Hok mRNA via its 5′-end single-stranded leader and competes with the 3′ end of Hok mRNA for binding to the *mok* translational initiation region. *EMBO J 13*:1960–1968.

Tomizawa J. 1990. Control of ColE1 plasmid replication. Interaction of Rom protein with an unstable complex formed by RNA I and RNA II. *J Mol Biol 212*:695–708.

Wagner EGH, Blomberg P, Nordström K. 1992. Replication control in plasmid R1: Duplex formation between the antisense RNA, CopA, and its target, CopT, is not required for inhibition of RepA synthesis. *EMBO J 11*:1195–1203.

Wagner EGH, Brantl S. 1998. Kissing and RNA stability in antisense control of plasmid replication. *Trends Biochem Sci 23*:451–454.

Wagner EGH, Simons RW. 1994. Antisense RNA control in bacteria, phages, and plasmids. *Annu Rev Microbiol 48*:713–742.

Walter F, Murchie AIH, Lilley DMJ. 1998a. Folding of the four-way RNA junction of the hairpin ribozyme. *Biochemistry 37*:17629–17636.

Walter F, Murchie AIH, Thomson JB, Lilley DMJ. 1998b. Structure and activity of the hairpin ribozyme in its natural junction conformation: Effect of metal ions. *Biochemistry 37*:14195–14203.

Weeks KM, Crothers DM. 1993. Major groove accessibility of RNA. *Science 261*:1574–1577.

Westhof E. 1993. Modeling the three-dimensional structure of ribonucleic acids. *J Mol Struct 286*:203–211.

Westhof E, Romby P, Romaniuk PR, Ebel JP, Ehresmann C, Ehresmann B. 1989. Computer modeling from solution data of spinach chloroplast and *X. laevis* somatic and oocyte 5S rRNAs. *J Mol Biol 207*:417–431.

Wilson IW, Praszkier J, Pittard AJ. 1993. Mutations affecting pseudoknot control of the replication of B group plasmids. *J Bacteriol 175*:6476–6483.

Zeiler BN, Simons RW. 1998. Antisense RNA structure and function. In: Simons RW, Grunberg-Manago M, eds. *RNA structure and function*. Cold Spring Harbor, New York: Cold Spring Harbor Laboratory Press. pp 437–464.